

Published in final edited form as:

Nat Neurosci. 2018 January ; 21(1): 19–23. doi:10.1038/s41593-017-0040-x.

Ca²⁺ activity signatures of myelin sheath formation and growth *in vivo*

Marion Baraban¹, Sigrid Koudelka¹, and David A Lyons¹

¹Centre for Neuroregeneration, Centre for Discovery Brain Sciences, University of Edinburgh, 49 Little France Crescent, Edinburgh EH16 4SB, UK

Abstract

During myelination, individual oligodendrocytes initially over-produce short myelin sheaths that are either retracted or stabilised. By live imaging oligodendrocyte Ca²⁺ activity *in vivo*, we find that high-amplitude long-duration Ca²⁺ transients in sheaths prefigure retractions, mediated by calpain. Following stabilisation, myelin sheaths grow along axons, and we find that higher frequency Ca²⁺ transient activity in sheaths precedes faster elongation. Our data implicate local Ca²⁺ signalling in regulating distinct stages of myelination.

Dynamic regulation of myelination by oligodendrocytes in the central nervous system (CNS) is essential for nervous system development and life-long function¹, but our understanding of myelin sheath formation and growth is limited. Zebrafish are well suited to studying the dynamics of CNS myelination *in vivo*, due to their capacity for non-invasive longitudinal imaging. Previous imaging studies using zebrafish have shown that individual oligodendrocytes initiate formation and elongation of their myelin sheaths within a critical period of about 5 hours^{2,3}, mirroring hours-long myelin sheath generation by mammalian oligodendrocytes *in vitro*⁴. During sheath formation, myelinating oligodendrocytes initially overproduce short myelin sheaths (circa 5µm in length), with some stabilised, and others fully retracted^{2,3,5,6}. Following stabilisation, myelin sheaths grow along and around associated axons³, to achieve dimensions that mediate the timing of impulse conduction and thus neural circuit function⁷. Although axonal signals, including neuronal activity, can regulate the formation and growth of myelin sheaths (e.g.5,8–10), the localised signalling mechanisms that control the dynamics of myelination by oligodendrocytes remain to be elucidated.

Users may view, print, copy, and download text and data-mine the content in such documents, for the purposes of academic research, subject always to the full Conditions of use:http://www.nature.com/authors/editorial_policies/license.html#terms

Correspondence prior to publication to David A Lyons (david.lyons@ed.ac.uk) and after publication to either David A Lyons or Marion Baraban (marion.baraban@ed.ac.uk).

Accession codes

The Genbank accession number for *calpastatin* mRNA is MG387170.

Author contributions

MB designed and performed experiments and co-wrote manuscript. SK performed experiments using chemical inhibitors. DAL designed experiments, managed project and co-wrote manuscript.

Competing financial interests

I declare that the authors have no competing interests as defined by Springer Nature, or other interests that might be perceived to influence the results and/or discussion reported in this paper.

Ca^{2+} is a second messenger that regulates many events, and localised Ca^{2+} activity has been observed in oligodendrocyte precursor cells¹¹, myelinating oligodendrocytes¹⁰, and even in mature myelin sheaths¹² *in vitro* and *ex vivo*. We reasoned that determining how localised Ca^{2+} activity relates to the formation and growth of myelin sheaths *in vivo* would provide novel insights into mechanisms of CNS myelination.

To visualise Ca^{2+} activity in myelinating oligodendrocytes, we used the genetically encoded calcium indicator GCaMP6s¹³, which we expressed in oligodendrocytes by crossing Tg(sox10:KalTA4) and Tg(uas:GCaMP6s) transgenic zebrafish lines (Online Methods). We imaged GCaMP6s expressing oligodendrocytes in the spinal cord of zebrafish larvae between 3-4 days post fertilisation (dpf), as myelin sheaths are being formed and starting to elongate^{2,3}. We first assessed the kinetics of individual localised Ca^{2+} transients in myelin sheaths by high-speed 2D (4Hz) imaging, and found that essentially all transients lasted longer than 3.5 seconds (Supplementary Fig. 1, Supplementary Movie 1). Therefore, we 3D imaged Ca^{2+} activity in all myelin sheaths belonging to individual oligodendrocytes with a time interval of 2.5 seconds (Fig. 1A-E, Online Methods, Supplementary Fig. 2, and Supplementary Movies 2 and 3).

To correlate Ca^{2+} activity with myelination, we time-lapse imaged individual GCaMP6s-expressing oligodendrocytes for multiple 20 minute blocks over a 5-9 hour period during which they initiated formation and elongation of their myelin sheaths (Fig. 1F,G). Prior to each Ca^{2+} imaging block, we acquired a high-resolution 3D z-stack of GCaMP6s-expressing oligodendrocytes together with sox10:mRFP, which allowed assessment of sheath morphology (Fig. 1F,G and see Online Methods). We quantified the Ca^{2+} activity of 305 sheaths of 18 oligodendrocytes in 18 animals. Analyses of 448 Ca^{2+} transients in the 187 sheaths that exhibited activity (out of the 305 sheaths imaged) revealed significant diversity in the frequency (Fig. 1H), amplitude and duration of transients between sheaths (Fig. 1I,J) (Median amplitude per sheath $F/F_0 = 0.7$, IQR=0.9; Median Ca^{2+} transient duration= 23s, IQR=17 seconds per sheath). We also found that duration and amplitude were positively correlated, whereby longer duration transients tended to also be of higher amplitude (Fig. 1K).

The diversity in Ca^{2+} transient activity between sheaths suggested that their frequency, duration and/or amplitude may influence myelination. We first focussed on the relationship between Ca^{2+} activity and myelin sheath formation. We found that 61 of the 305 sheaths analysed were completely retracted during our imaging protocol, reflecting the initial over-production of sheaths. Intriguingly, we found that the amplitude of Ca^{2+} transients in sheaths that were subsequently retracted was three-fold higher than in those sheaths that were stabilised (Fig. 2A,B,D: Median amplitude =1.8 F/F_0 in fully retracted sheaths vs 0.6 F/F_0 in stabilised sheaths). Furthermore, we observed an increase in Ca^{2+} transient duration in sheaths that were subsequently retracted (Fig. 2C,D: Median duration= 35s in retracted sheaths vs 22s in stabilised). Interestingly, the Ca^{2+} transients observed in sheaths that were subsequently retracted travelled from sheath to process (Supplementary Fig. 3, Supplementary Movie 4), reflecting the directionality of retraction, first of the sheath and then the process (Fig. 2A, Supplementary Fig. 4). These observations lead us to hypothesise

that localised high-amplitude long-duration Ca^{2+} transients may mediate sheath retraction through activation of Ca^{2+} -dependent mechanisms.

We hypothesised that calpain enzymes, Ca^{2+} dependent non-lysosomal proteases, might mediate sheath retraction. Calpains underpin many aspects of cellular breakdown, including the localised pruning of dendrites in *Drosophila* following large Ca^{2+} transients¹⁴. To test whether calpain mediates myelin sheath retractions, we took chemical and genetic approaches. We first treated animals with the calpain inhibitor PD15060615 from 2-4 dpf, and assessed the morphology of individual oligodendrocytes with mbp:mCherry-CAAX 6. We found that PD150606 treatment increased myelin sheath number per oligodendrocyte (Fig. 2E,H) (Average sheath number per oligodendrocyte: DMSO 14.4 ± 3.2 vs PD150606 18.7 ± 5.9). In order to whether calpain actually mediates retraction of sheaths, we carried out time-lapse microscopy of PD150606-treated animals. These studies revealed a lower rate of sheath retraction in calpain-inhibited animals during the dynamic period of sheath stabilisation and retraction (Fig. 2F,I and Supplementary movies 5+6) (Sheath retraction per oligodendrocyte per hour, DMSO 0.34 ± 0.13 vs PD150606 0.24 ± 0.13). To independently and cell autonomously test the role for calpain in regulating myelin sheath number, we expressed the endogenous inhibitor of calpain, calpastatin16, in myelinating oligodendrocytes (see Online Methods and Supplementary Fig. 5). Analysis of oligodendrocyte morphology revealed that cell-type specific disruption of calpain protease function increased the number of myelin sheaths compared to control (Fig. 2G,J) (Average sheath number per cell mbp:meGFP 15.8 ± 6.4 vs mbp:meGFP-calpastatin 20.5 ± 5.8).

Together, these data support our imaging-driven hypothesis that calpain regulates retraction of myelin sheaths during the dynamic period of myelin sheath formation by individual oligodendrocytes.

We next assessed how Ca^{2+} transient activity might relate to myelin sheath growth. By comparing Ca^{2+} activity and differential growth over time (Fig. 3A,B), we found that the frequency of the lower amplitude shorter duration Ca^{2+} transients observed in stabilised sheaths correlated positively with the speed of sheath elongation (Fig. 3C,D). Interestingly, when we analysed how individual sheaths grew after each Ca^{2+} transient, we observed positive elongation within the first 2 hours of the Ca^{2+} transient (Fig. 3E). We did not see any correlation between the average amplitude or duration of transients with the speed of growth (Supplementary Fig. 6). These observations show the frequency of low amplitude short duration Ca^{2+} transients in stabilised sheaths is predictive of their speed of elongation, suggesting that dynamic changes in myelin sheath Ca^{2+} concentration regulate sheath growth.

Our live imaging has revealed distinct signatures of localised Ca^{2+} activity during CNS myelination. High-amplitude long duration Ca^{2+} transients precede localised retraction of sheaths, mediated by calpain, whereas the frequency of lower amplitude shorter duration transients in stabilised sheaths correlates positively with their speed of elongation (Summarised in Supplementary Fig. 7). How could distinct Ca^{2+} signatures lead to such different outcomes during myelination? With respect to sheath retraction, it is known that different isoforms of calpain have distinct sensitivities to Ca^{2+} concentration, with some

primed for activation by localised changes in Ca^{2+} concentration¹⁷. It is possible that large localised increases in Ca^{2+} concentration following individual high-amplitude long-duration transients could stimulate local protease activity that leads to sheath retraction, e.g. by localised degradation of cytoskeletal components. With respect to the speed of sheath elongation, it is now known that myelin sheath growth occurs is driven at inside of the myelin sheath³, at least in part, by iterative cycles of actin polymerisation and depolymerisation¹⁸. Given that actin polymerisation/depolymerisation can be regulated by Ca^{2+} , it is possible that localised changes in Ca^{2+} concentration could affect the speed of sheath growth via regulating the actin cytoskeleton.

Many additional questions remain as to how localised Ca^{2+} regulates myelination. Which signal(s) lead to the distinct changes in myelin sheath Ca^{2+} during retraction, stabilisation and growth? Neuronal activity is one signal known to affect myelination^{5,8–10}, and many of its candidate mediators in oligodendrocytes converge on regulation of intracellular Ca^{2+} ¹⁹. Indeed, a complementary study to ours indicates that neuronal activity regulates about half of the Ca^{2+} transients in myelin²⁰. How Ca^{2+} might affect ongoing sheath growth and remodelling throughout life, and during regeneration, also remain to be investigated. We anticipate that live Ca^{2+} imaging-focussed approaches will continue to elucidate the mechanisms underlying the dynamic regulation of myelination in the CNS.

Online Methods

Zebrafish husbandry

All animal studies were carried out with approval from the UK Home Office and according to its regulations, under project licenses 60/ 8436 and 70/8436. The project was approved by the University of Edinburgh Institutional Animal Care and Use Committee. We used zebrafish (*Danio rerio*) only, and the following transgenic lines in this study: tg(sox10(7.2):KalTA4GI)21, tg(UAS:mem-GFP), tg(uas:GCaMP6s)13 and tg(sox10:mRFP)22. All Ca^{2+} imaging was carried out in the nacre background²³, which lack melanocytes.

Image acquisition

We combined stable transgenic zebrafish Tg(sox10:KalTA4), which drives gene expression in the oligodendrocyte lineage, with Tg(uas:GCaMP6s) that expresses the genetically encoded calcium indicator GCaMP6s under the control of 14X repetitive Upstream Activator Sequences (uas), the nacre homozygous mutant line that lacks melanocytes, and also Tg(sox10:mRFP) which drives membrane localised RFP expression in the myelinating oligodendrocyte lineage. The combination of Tg(sox10:KalTA4) and Tg(uas:GCaMP6s) leads to mosaic expression of GCaMP6s in isolated cells of the oligodendrocyte lineage in the CNS.

Prior to imaging, larvae were screened for the expression of GCaMP6s in isolated oligodendrocytes in the dorsal spinal cord at 3-4 days post fertilisation (dpf). Selected larvae were paralysed using the Neuromuscular Junction (NMJ) blocking nicotinic receptor antagonist pancuronium bromide (Sigma, P1918), which was dissolved in embryo medium

(0.15-0.3mg/ml). Larvae were then embedded in 1.3% agarose for imaging. Imaging was carried out on an Olympus Revolution XDi spinning disk confocal microscope using a 1.2 NA 60X water immersion objective, plus a camera zoom of 2X, giving an X-Y image area of 117x117 μ m and acquisition at 512x512 pixels. Larvae were maintained at 28°C in temperature controlled chamber (Okolab). Images were acquired using the iQ3 software (Andor) and iXon EMCCD Ultra 897 camera.

For initial 2D characterisation of calcium transient kinetics, Tg(sox10:KalTA4, uas:GCaMP6s), Tg(sox10:mRFP) larva were time-lapse imaged for periods of 10-30 min with 100ms exposure time, and 150-250ms intervals, reflecting imaging in one (GCaMP6s) or two (GCaMP6s and mRFP) channels, for a final rate of 4-6.66 Hz (final rates also incorporate camera integration times).

To investigate how Ca²⁺ activity related to cell fate, Tg(sox10:KalTA4, uas:GCaMP6s, sox10:mRFP), *nacre*^{-/-} larva were imaged every 60-120 min as follows. First, one high-resolution 3D 29 μ m deep (average \pm 2 μ m) z-stack of both RFP and GCaMP6s expression was acquired at 100ms exposure, 4x averaging, and z-intervals between optical slices of 0.33 μ m. Immediately thereafter, 3D time-lapse images of GCaMP6s expression alone were acquired of the same 29 μ m (\pm 2 μ m) volume, at 100ms exposure (no averaging), and z step of 1.3 μ m. The time interval between consecutive z-stacks in the time-lapse was 2.538s (\pm 0.264s), including z-positioning and camera integration times. Absolute values of imaging parameters were incorporated into analyses of all individual Ca²⁺ transients and time-lapse data.

Image analysis

2D time-lapse imaging data were analysed using Fiji. To correct for sample drift throughout the movie we used the “Image stabilizer registration” Fiji plugin (Kang Li). Because of the very sparse labelling of individual GCaMP6s expressing oligodendrocytes it is possible to identify Ca²⁺ transients by manual inspection of time-lapse series. Regions of interest are then applied around all myelin sheaths and also in a separate area with no GCaMP6s expression, which represents background. Then fluorescent intensity measurements are extracted from both ROIs and imported into Excel. To measure F/F_0 we apply the following formula: $F/F_0 = (F(t) - F(0)) / (F(0) - F(\text{background}))$ where $F(t)$ is the fluorescence intensity in the ROI in which the Ca²⁺ transient was observed at time (t), $F(0)$ the average fluorescence intensity of the first 4 frames of the movie in the same ROI and $F(\text{background})$ the fluorescence intensity of the background ROI at time (t). See Supplementary Figure 1 for overview. This F/F_0 information and corresponding image acquisition parameters are imported into pClamp (Molecular Devices) for detailed analyses of the duration and amplitude of individual Ca²⁺ transients.

For 3D time-lapse imaging data, maximum intensity projections of the individual time-points from 3D time-lapse data were made using Fiji and the image stabilizer Fiji plugin was again run to account for drift. In parallel 3D datasets were registered using the “Descriptor-based series registration (2d/3d+t)” Fiji plugin, after which maximum intensity projections are made and Ca²⁺ transients identified manually. Ca²⁺ transients were then identified manually. Only Ca²⁺ transients identified following both modes of image processing were

considered as valid. All myelin sheaths without overlapping structures in the X-Y or Z planes were analysed. Regions of interest are then applied around all myelin sheaths and corresponding background, as above. In addition, the ROI with the candidate Ca²⁺ transient was moved to an immediately adjacent region in order to rule out the possibility that any, very infrequent, general increase in background fluorescence in the region could identify a spurious transient. Key parameters for analysis of 3D time-lapse datasets were extracted from the iQ3 metadata files using a custom-written Fiji macro written by Dr. Bertrand Vernay, University of Edinburgh. These parameters were then imported into Microsoft Excel for analysis. All Ca²⁺ transients were identified by $\Delta F/F(0)$ as above and analysed using pClamp.

To measure myelin sheath length, we used the 3D high-resolution single time z-stack datasets acquired before each period of GCaMP6s time-lapse imaging. The expression of GCaMP6s allowed identification of individual myelin sheaths and the membrane localised mRFP in the same sheaths allowed more accurate measurement of length.

Calpain inhibitor treatment and analysis

The calpain inhibitor PD150606 (Tocris) was applied in solution from 50 μ M -75 μ M with 1% DMSO to embryos from 2-4 dpf and vehicle alone applied to controls. The morphology of myelinating oligodendrocytes was assessed as previously by imaging individual oligodendrocytes expressing the mbp:mCherry-CAAX reporter⁶. Images of individual myelinating oligodendrocytes were taken on a Zeiss 880 with Airyscan, in animals immobilized using 1.3% Low melting point agarose with 0.03% Tricaine in embryo medium. Individual myelin sheaths were identified in 3D z-stacks and measured using Fiji. Time-lapse analyses were carried out using tg(sox10(7.2):KalTA4GI), tg(UAS:mem-GFP), animals, which were imaged on a Zeiss 880 Airyscan in Fast Mode and with a piezo z-drive to allow rapid acquisition of confocal z-stacks. Z-stack images were collected every 5 minutes for a 15 hour period from 81-96 hpf.

Cell-type specific expression of calpastatin in myelinating oligodendrocytes

In order to disrupt calpain function in a cell type specific manner, we chose to express the endogenous inhibitor of calpain, calpastatin²⁴, in myelinating oligodendrocytes. We first cloned zebrafish calpastatin. To do so, we extracted mRNA from whole zebrafish embryos at 3 and 4 dpf, generated cDNA and amplified calpastatin using the following primers castF: 5'-ATGGCGTACGCAATGTATTGG-3'; castR: 5'-TTATCTTTTTCCAGCCTTTGTGG-3' and high fidelity Phusion polymerase (Thermo Fisher). We cloned cast fragments into pCRTM-Blunt II-TOPOTM (Thermo Fisher) and Sanger sequenced clones (Source Bioscience). We subcloned multiple cast mRNA variants into pCS2+ and generated synthetic mRNA, which we injected into animals at the one cell stage to identify full-length version that lead to an increase in myelin sheath number per oligodendrocyte in the dorsal spinal cord (Supplementary Fig. 5 and data not shown). We next generated a p3E vector in which full length cast was flanked by p2A and a SV40 polyA sequences. We then generated a pME vector with the Fyn myristoylation domain added to GFP, by amplifying GFP from pCS2+eGFP and adding the myristoylation sequence using the following primer meGFPF 5'-ATGGGCTGTGTGCAATGTAAGGATAAAGAAGCAACAAAAGTACG-3.' To

generate a construct for cell type specific expression of meGFP-pA or meGFP-2A-cast-pA we recombined the previously described p5E-mbp plasmid containing zebrafish myelin basic protein regulatory sequence²⁵, with the pME-meGFP and p3E-pA or with the pME-meGFP and p3E-2A-cast-pA. mbp:meGFP-pA (5pg) or mbp:meGFP-2A-cast-p2A (10pg) plasmids were injected into zebrafish at the 1-2 cell stage together with 25pg tol2 mRNA²⁶. Individual oligodendrocytes were imaged at 4dpf using meGFP on a Zeiss 880 Airyscan confocal microscope in Fast Mode.

Statistics and reproducibility

All data are shown as mean \pm standard deviation or median with 1st and 3rd quartiles as indicated. Please see Supplementary table 1 for data on confidence levels and intervals related to raw data. All statistical tests were carry out using GraphPad (Prism 6 or 7). Power calculations were calculated using Statemate 2 to determine for Ca²⁺ imaging analyses, and investigations of the role of calpain signalling in myelination. All analyses had a power >80%. Randomisation of imaging and analyses was not carried out on animals whose myelin sheaths were Ca²⁺ imaged, as all are wildtype. For chemical and genetic manipulations of calpain function, zebrafish embryos for both experimental and control conditions derived from the same clutch (per experiment). For time-lapse analyses of chemical inhibitor treated animals, control and experimental animals were imaged separately for technical reasons. Embryos were grown up in the same incubator and the same conditions prior to analyses, all live imaging. During live imaging analyses, experimental and control animals were imaged in an alternating pattern (per experiment) to ensure no confounding effects of stage of development between groups. The analysis of all experimental findings were carried out blinded and image data was randomised using a custom-made script.

The data shown in Supplementary Figure 1 is representative of 20 myelin sheaths imaged in 12 animals over 4 separate experimental sessions.

The data shown in Figure 1A-E and Supplementary Figure 2 are representative of 40 oligodendrocytes imaged in 40 animals over 25 separate occasions.

The images analysed and data presented in Figures 1G-K, 2A-D and Figure 3 are representative of 18 cells imaged over 9 separate experimental sessions.

The images analysed and data presented in Figure 2E,H are representative of 4 experimental sessions.

The images analysed and data presented in Figure 2G,J are representative of 4 experimental sessions.

The images analysed and data presented in Figure 2F,I are representative of 6 experimental sessions.

Data were tested for normality by the D'Agostino & Pearson omnibus normality test. Normal distributed data were tested as appropriate by two-tailed student's t-test unpaired (equal variance was tested using the F test) or two-tailed one-way ANOVA (equal variance

was tested using the Brown-Forsythe test). Non-normally distributed data were tested by a two-tailed Mann-Whitney tests. The Pearson's correlation test was used to test the correlation in Fig.1J and Fig. 3D. Linear regression analyses were used to test whether the slopes differed significantly from zero in Fig. 3E. Throughout all analyses * $p < 0.05$, ** $p < 0.01$, *** $p < 0.001$, **** $p < 0.0001$.

Please see Life Sciences Reporting Summary for further details on experimental design.

Data and code availability

Transgenic constructs and transgenic zebrafish lines will be available upon request. The data that support the findings of this study are available from the corresponding author upon reasonable request. Custom written code for analyses of Ca²⁺ imaging data are specific to the imaging platform, but details are available upon request. A custom written code for blinding of image analyses in Fiji/ImageJ is available as a supplementary software item.

Supplementary Material

Refer to Web version on PubMed Central for supplementary material.

Acknowledgements

We would like to thank members of the Lyons lab, as well as Thomas Becker, Peter Brophy, Charles French-Constant, Matthew Livesey, Dies Meijer, Will Talbot and Claire Wyart for helpful comments on the manuscript. We would like to thank Herwig Baier for transgenic zebrafish, Bertrand Vernay for support in image analysis. This work was supported by a Lister Institute Research Prize and a Wellcome Trust Senior Research Fellowship (102836/Z/13/Z) to DAL.

References

1. Chang K-J, Redmond SA, Chan JR. *Nat Neurosci.* 2016; 19:190–197. [PubMed: 26814588]
2. Czopka T, French-Constant C, Lyons DA. *Developmental Cell.* 2013; 25:599–609. [PubMed: 23806617]
3. Snaidero N, et al. *Cell.* 2014; 156:277–290. [PubMed: 24439382]
4. Watkins TA, Emery B, Mulinyawe S, Barres BA. *Neuron.* 2008; 60:555–569. [PubMed: 19038214]
5. Hines JH, Ravanelli AM, Schwandt R, Scott EK, Appel B. *Nat Neurosci.* 2015; 18:683–689. [PubMed: 25849987]
6. Mensch S, et al. *Nat Neurosci.* 2015; 18:628–630. [PubMed: 25849985]
7. Fields RD. *Nat Rev Neurosci.* 2015; 16:756–767. [PubMed: 26585800]
8. Wake H, et al. *Nature Communications.* 2015; 6:7844.
9. Koudelka S, et al. *Curr Biol.* 2016; 26:1447–1455. [PubMed: 27161502]
10. Wake H, Lee PR, Fields RD. *Science.* 2011; 333:1647–1651. [PubMed: 21817014]
11. Sun W, Matthews EA, Nicolas V, Schoch S, Dietrich D. *Elife.* 2016; 5
12. Micu I, et al. *Experimental Neurology.* 2016; 276:41–50. [PubMed: 26515690]
13. Chen T-W, et al. *Nature.* 2013; 499:295–300. [PubMed: 23868258]
14. Kanamori T, et al. *Science.* 2013; 340:1475–1478. [PubMed: 23722427]
15. Wang KK, et al. *PNAS.* 1996; 93:6687–6692. [PubMed: 8692879]
16. Moldoveanu T, Gehring K, Green DR. *Nature.* 2008; 456:404–408. [PubMed: 19020622]
17. Campbell RL, Davies PL. *Biochem J.* 2012; 447:335–351. [PubMed: 23035980]
18. Nawaz S, et al. *Developmental Cell.* 2015; 34:139–151. [PubMed: 26166299]
19. Pitman KA, Young KM. *Int J Biochem Cell Biol.* 2016; 77:30–34. [PubMed: 27233230]

21. Almeida RG, Lyons DA. *Zebrafish*. 2015; 12:377–386. [PubMed: 26485616]
22. Kirby BB, et al. *Nat Neurosci*. 2006; 9:1506–1511. [PubMed: 17099706]
23. White RM, et al. *Cell Stem Cell*. 2008; 2:183–189. [PubMed: 18371439]
24. Kiss R, Kovács D, Tompa P, Perczel A. *Biochemistry*. 2008; 47:6936–6945. [PubMed: 18537264]
25. Almeida RG, Czopka T, Ffrench-Constant C, Lyons DA. *Development*. 2011; 138:4443–4450. [PubMed: 21880787]
26. Kwan KM, et al. *Dev Dyn*. 2007; 236:3088–3099. [PubMed: 17937395]

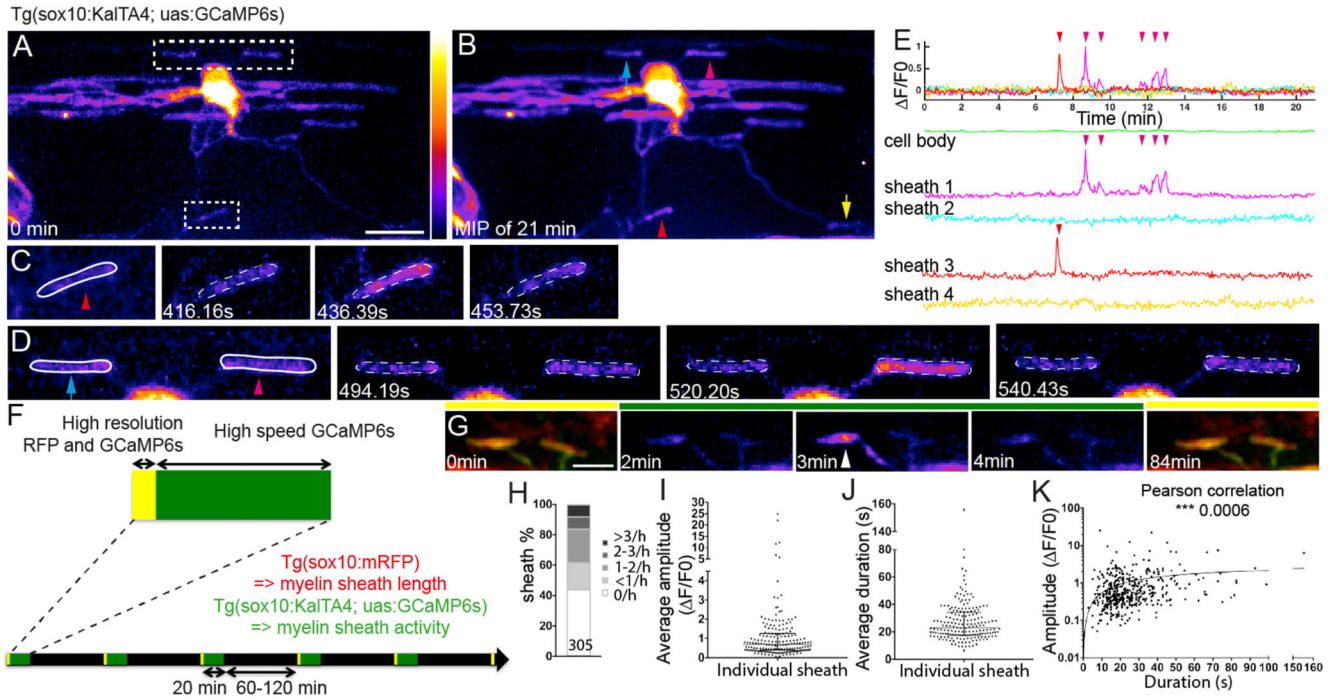


Figure 1. Live imaging reveals localised Ca^{2+} activity in newly forming myelin sheaths

A. Maximum intensity projection of a 3D z-stack of the first time-point from a 21 minute-long movie of a GCaMP6s expressing oligodendrocyte. Two areas of interest indicated, top corresponding to D and bottom to C. Scale bar= 10 μm . Fire LookUpTable reflects grey value range 0-65,535 (black to white).

B. Maximum intensity projection of all time-points of cell shown in A. Arrowheads indicate sheaths with increased fluorescence, reflecting Ca^{2+} activity during the movie. Arrows point to sheaths with no increase.

C, D, myelin sheaths demarcated within ROIs outlined in A, at indicated times.

E. F/F_0 over time. Arrowheads indicate sheaths shown in corresponding colours in B, C and D.

F. Schematic of time-lapse imaging experiment with interspersed imaging of cell morphology (yellow) and Ca^{2+} (green).

G. Sample images of myelin sheath morphology (under yellow bars) with intervening periods of Ca^{2+} imaging (under green bar). Arrowhead points to Ca^{2+} transient in sheath. Scale bar=5 μm .

H. Distribution of Ca^{2+} transient frequencies of 305 sheaths, analysed in 18 animals.

I. Distribution of average Ca^{2+} transient amplitude per sheath (187 sheaths from 18 animals). Graph shows median and 1st and 3rd quartiles.

J. Distribution of average Ca^{2+} transient duration per sheath (187 sheaths from 18 animals). Graph shows median and 1st and 3rd quartiles.

K. Correlation between amplitude and duration per individual Ca^{2+} transient events (448 events from 187 sheaths in 18 animals, Pearson's Correlation Test, $p=0.0006$).

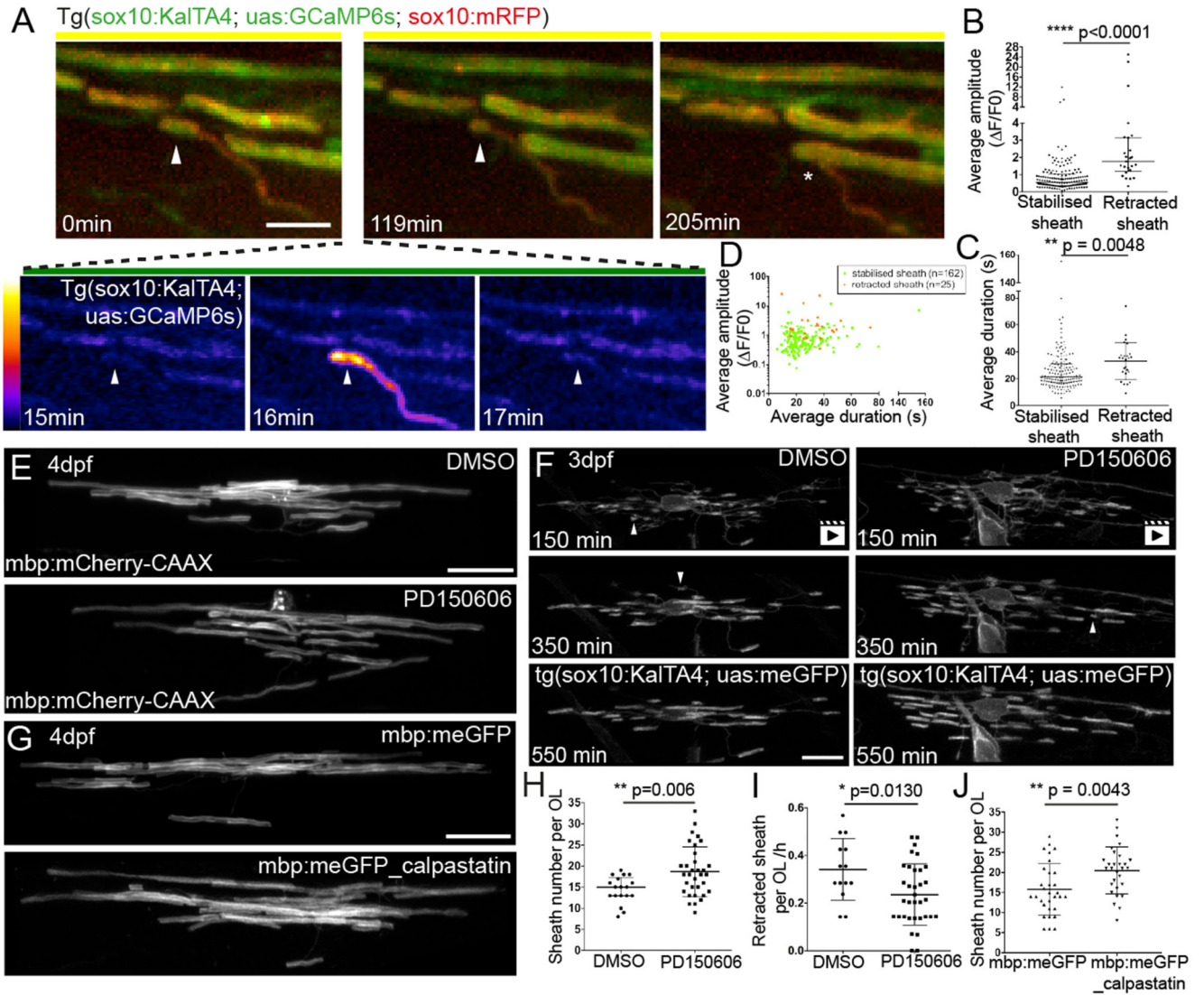


Figure 2. High-amplitude long duration Ca^{2+} transients precede calpain-driven sheath retractions.

A. Frames from a time-lapse imaging experiment. The myelin sheath imaged in high-resolution mode (0 min) exhibits a Ca^{2+} transient 16 minutes into a period of high-speed GCaMP6s imaging (see also Supplementary Fig. 3) subsequently retracts, first along the length of the axon (119 min) and then entirely from the axon (205 min, asterisk). Scale bar=5 μ m. Fire LookUpTable reflects grey value range 0-65,535 (black to white).

B. Average amplitude of Ca^{2+} transients in sheaths that are either stabilised or fully retracted (n=25 retracted sheaths, 12 animals and n=162 stabilised sheaths, 18 animals; Graph shows median and 1st and 3rd quartiles. Two-tailed Mann-Whitney test, $p < 0.0001$).

C. Average duration of Ca^{2+} transients in sheaths shown in B. Graph shows median and 1st and 3rd quartiles. Two-tailed Mann-Whitney test, $p = 0.0048$.

D. Average amplitude and average duration of transient events in sheaths that are stabilised (green) or fully retracted (orange).

E. mbp:mCherry-CAAX expressing oligodendrocytes in control (top) and PD150606 treated animal (bottom) at 4 dpf. Scale bar= 10 μ m. Quantitation in 2H.

F. Frames from time-lapse movies of oligodendrocytes during myelination in a DMSO treated (left) and PD150606 treated (right) animal. Arrowheads point to sheaths that are retracted. See also Supplementary Movies 5+6. Scale bar= 10 μ m. Quantitation in 2I.

G. mbp:meGFP expressing oligodendrocytes (top) and mbp:meGFP-calpastatin (bottom) at 4 dpf. Scale bar= 10 μ m. Quantitation in 2J.

H. Myelin sheath number per oligodendrocyte in DMSO and PD150606 treated animals (n=18 OLs from 18 DMSO-treated animals; n= 33 OLs from 33 PD150606-treated animals; Graph shows mean and SD. Two-tailed t-test, p=0.006).

I. Rate of myelin sheath retraction per hour in DMSO and PD150606 treated animals as analysed by time-lapse microscopy. (n=14 OLs from 14 DMSO-treated animals and 34 OLs from 34 PD150606-treated animals. Graph shows mean and SD. Two-tailed t-test, p=0.013).

J. Myelin sheath number per mbp:meGFP and mbp:meGFP-calpastatin expressing oligodendrocytes at 4 dpf. (n=31 OLs in 22 mbp:meGFP control animals, and n=29 OLs in 23 mbp:meGFP-calpastatin animals. Graph shows mean and SD. Two-tailed t-test, p=0.0043).

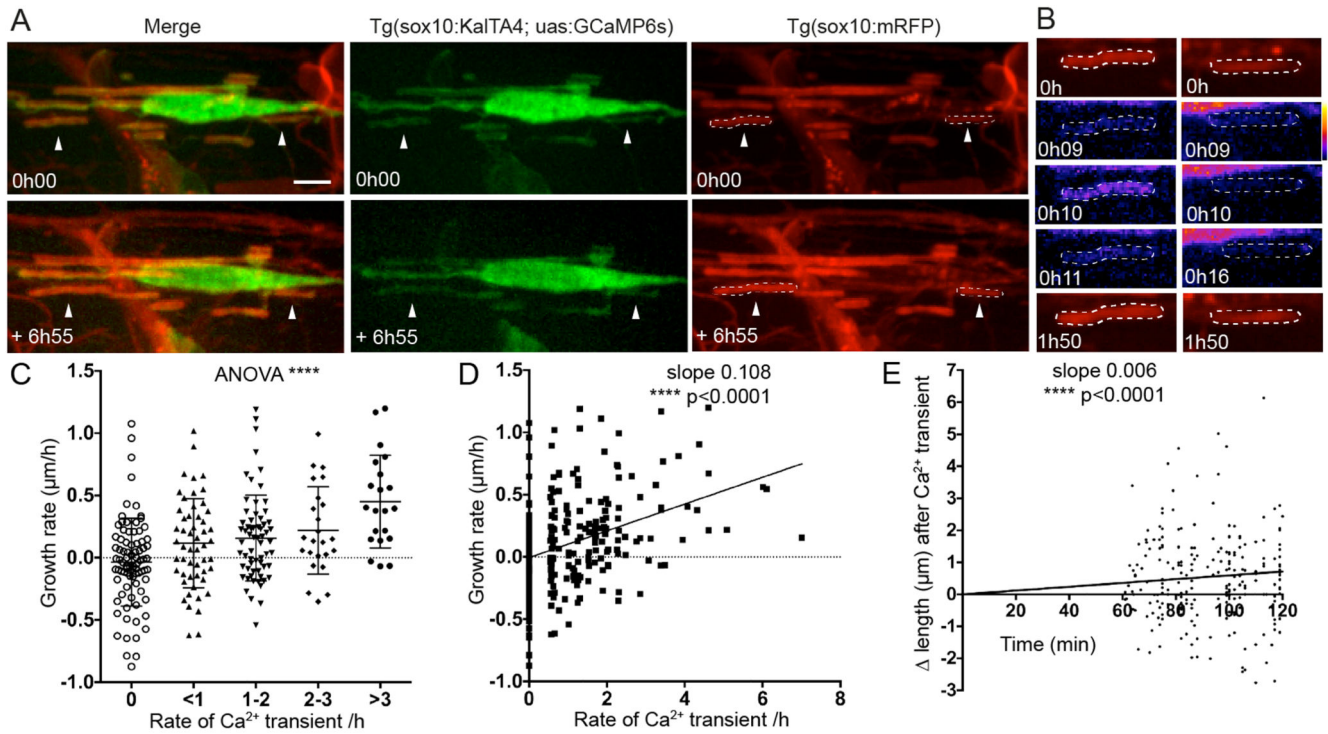


Figure 3. Ca^{2+} transient frequency correlates with sheath elongation

A. Images of a GCaMP6s expressing oligodendrocyte in a Tg(sox10:mRFP) background allows analysis of the growth and Ca^{2+} activity of individual isolated myelin sheaths, e.g. arrowheads over time. Top panels show initial time-point and bottom the same cell at the end of the movie almost 7 hours later. Scale bar= $5\mu\text{m}$.

B. Myelin sheaths indicated by arrowheads in A are outlined by ROIs and imaged over time. Note the Ca^{2+} transient at 0h 10 time-point in the sheath in the left column subsequently elongates.

C. Growth rate of myelin sheaths ($\mu\text{m}/\text{h}$) related to number of Ca^{2+} transients per hour. (ANOVA $p < 0.0001$, $F = 9.225$. Two-tailed unpaired t-test, 0 vs >3 transients/h $p < 0.0001$, 0 vs 2-3 transients/h $p = 0.0024$, 0 vs 1-2 transients/h $p = 0.0011$, 0 vs <1 transient/h $p = 0.0162$, <1 vs >3 transients/h $p = 0.0006$, 1-2 vs >3 transients/h $p = 0.0014$, 2-3 vs >3 transients/h $p = 0.0376$; 0 transient/h $n = 82$ sheaths from 17 animals, <1 transient/h $n = 53$ from 16 animals, 1-2 transients/h $n = 64$ sheaths from 17 animals, 2-3 transients/h $n = 24$ sheaths from 11 animals, >3 transients/h $n = 21$ sheaths from 11 animals). Graph indicates means and standard deviations.

D. Scatterplot analysis of growth rate of myelin sheaths ($\mu\text{m}/\text{h}$) related to number of Ca^{2+} transients per hour (Slope= 0.108. Pearson's Correlation Test, $p < 0.0001$, $n = 244$ sheaths).

E. Change in sheath length over time following 324 Ca^{2+} transients, with the time of all transients set as time 0 (slope 0.006, Linear Regression test, $p < 0.0001$).